

Correlated Electronic Properties of a Graphene Nanoflake: Coronene

Suryoday Prodhan,^{1, a)} Sumit Mazumdar,^{2, 3, b)} and S. Ramasesha^{1, c)}

¹⁾*Solid State and Structural Chemistry Unit, Indian Institute of Science, Bangalore-560012, India.*

²⁾*Department of Physics, University of Arizona, Tucson, Arizona 85721, USA.*

³⁾*College of Optical Sciences, University of Arizona, Tucson, Arizona 85721, USA.*

(Dated: 16 January 2021)

We report studies of the correlated excited states of coronene and substituted coronene within the Pariser-Parr-Pople (PPP) correlated π -electron model employing symmetry adapted density matrix renormalization group technique. These polynuclear aromatic hydrocarbons can be considered as graphene nanoflakes. We review their electronic structures utilizing a new symmetry adaptation scheme that exploits electron-hole symmetry, spin-inversion symmetry and end-to-end interchange symmetry. Study of the electronic structures sheds light on the electron correlation effects in these finite-size graphene analogues, which diminishes on going from one-dimensional to higher-dimensional systems, yet is significant within these finite graphene derivatives.

Keywords: Symmetrized DMRG; Strongly Correlated System; Carbon Nanodots; Pariser-Parr-Pople (PPP) Model; Low-lying Excited States.

I. INTRODUCTION

In quantum chemical calculations of electronic structures of carbon (C)-based π -conjugated systems, the effects of electronic correlation have been probed by employing a number of techniques, most of which are variants of the restricted configuration interaction technique. Singles configuration interaction (SCI) based techniques suffice for studying one-photon optical gaps in neutral carbon-based molecular systems, as these excitations are predominantly single electron-hole excitations¹. However, for strongly correlated low-dimensional systems, the shortcomings of the SCI are also well-documented²⁻¹⁰. Time-dependent density functional theory¹¹⁻¹³ or GW approximation accompanied by Bethe-Salpeter correction¹⁴⁻¹⁷ are essentially equivalent to the SCI approximation as only two-particle (one electron - one hole) interactions are included in these approaches and higher-order CIs are excluded.

While full CI (FCI) study is the most preferred one, its use has been limited to ~ 18 -electron neutral systems, as the Hilbert space dimension increases exponentially with system size. Ab initio quantum chemical methods like CASPT2 that are able to reproduce the energy spectra of correlated π -electron molecules correctly are limited to 8 – 10-electron neutral systems¹⁸⁻²². Multiple reference singles and doubles CI (MRSDCI) approach is another suitable iterative method for introduction of higher-order CI effects but the Hilbert space dimensions for different excited states, for similar accuracy,

vary significantly^{6,7,23,24}. On the other hand, the Density Matrix Renormalization Group (DMRG) method, introduced by White, is an accurate numerical many-body technique for studying low-lying states of one and quasi-one dimensional systems in real space²⁵⁻²⁹. In the DMRG method, similar to other renormalization group methods, the Hilbert space dimension remains fixed independent of the system sizes. For discrete molecular systems with energy gaps, the area law of entanglement entropy also holds leading to high accuracy in the DMRG calculations^{27,28}, even with moderate dimensionality of block state space.

The DMRG scheme, as usually implemented, utilizes conservation of the number of particles and the z -component of the total spin S_z . Thus, in this scheme, a few low-lying states are obtained in each of the sectors with a fixed number of particles and fixed S_z value. Although schemes that exploit other symmetries have been developed, they are limited to a few orbitals and a few particles. Yet, in studies of π -conjugated systems that probe the lowest-energy dipole-connected state, the lowest two-photon state and the lowest triplet state, we need to exploit other symmetries like the electron-hole ($e-h$) symmetry, the spin-inversion symmetry and the end-to-end interchange symmetry (see below). However, although application of the DMRG technique or its symmetrized versions is straightforward in one- and quasi-one dimensional systems, it is not so trivial in higher dimensional systems like in graphene nanoflakes and graphene nanoribbons. Study of these large finite graphene analogues is expected to shed light on the properties in the thermodynamic limit and the effect of electronic correlation in these industrially important two-dimensional systems. Most of the earlier studies on graphene and graphene analogues have been done within non-interacting model or employing restricted configuration interaction technique with a few frontier molecular

^{a)}Current address: Laboratory for Chemistry of Novel Materials, University of Mons, Mons-7000, Belgium.; Electronic mail:suryodayp@iisc.ac.in

^{b)}Electronic mail:sumit@physics.arizona.edu

^{c)}Electronic mail:ramasesh@iisc.ac.in

orbitals^{30–51}, while the importance of electron correlation in the electronic and magnetic structures of these systems have been emphasized in recent studies^{23,24,52,53}. In the present paper, we demonstrate the application of symmetrized DMRG technique in the study of a graphene nanoflake, coronene, within a long-range correlated π -electron model. This molecule has recently been studied employing the MRSDCI approach^{23,24,54} and we reexamine the earlier results. We also study the effect of weak donor-acceptor substitutions which lowers the symmetry of the overall molecule. Transition dipole moments to the low-lying optical states along with two-photon absorption cross-sections for the low-lying two-photon states are also calculated.

The paper is organized as follows. In the next section, we have given an account of the model Hamiltonian employed in our study along with a brief discussion about the DMRG technique and the symmetries utilized in our calculations. In section III, we present our results for coronene and substituted coronene. In the last section we present our conclusions.

II. METHODOLOGY

Ab-initio DMRG calculations for neutral systems employing molecular orbitals have bottlenecks since the calculation of two-electron integrals are computationally expensive and consequently these studies employ ~ 50 active space orbitals⁵⁵. On the other hand, DMRG calculations with localized orbitals have been successfully employed for π -conjugated systems with several hundred p_z orbitals within the PPP Hamiltonian^{53,56–59}. Ab-initio study of arenes using the DMRG method has also revealed that fully localized orbitals bring about faster convergence of energies compared to canonical Hartree-Fock orbitals or split-localized orbitals⁵⁵, making the localized description as the picture of choice.

A. Model Hamiltonian

We consider the PPP π -electron Hamiltonian^{60,61} which is a widely employed semi-empirical model for studying the behavior of C-based π -conjugated systems^{3–9}. The PPP Hamiltonian is given by,

$$\hat{H} = \sum_{\langle i,j \rangle, \sigma} t_0 (\hat{c}_{i,\sigma}^\dagger \hat{c}_{j,\sigma} + \text{H.C.}) + \sum_i \epsilon_i \hat{n}_i + \sum_i \frac{U}{2} \hat{n}_i (\hat{n}_i - 1) + \sum_{i>j} V_{ij} (\hat{n}_i - z_i) (\hat{n}_j - z_j) \quad (1)$$

In the above $\hat{c}_{i,\sigma}^\dagger$ ($\hat{c}_{i,\sigma}$) creates (annihilates) a π -electron with spin σ on the p_z orbital on C-atom i ; $\hat{c}_{i,\sigma}^\dagger \hat{c}_{i,\sigma}$ is the corresponding number operator and $n_i = \sum_\sigma c_{i,\sigma}^\dagger \hat{c}_{i,\sigma}$ is

the total number operator. Here t_0 is the transfer integral between bonded C-atoms i and j , ϵ_i is the site energy of the i -th C-atom, U the repulsive Hubbard interaction between two electrons occupying the same p_z orbital, and V_{ij} is the long-range electron correlation between C-atoms i and j . The latter is obtained from the Ohno interpolation scheme^{62,63} (Eq. 2),

$$V_{ij} = 14.397 \left[\left(\frac{14.397}{U} \right)^2 + r_{ij}^2 \right]^{-\frac{1}{2}} \quad (2)$$

where the distance r_{ij} between the C-atoms i and j are in Å units while the Hubbard interaction energy term U is in electron-volts (eVs). Finally, z_i is the local chemical potential, expressed by the number of π -electrons on C-atom i which leaves the site neutral ($z_i = 1$ for C-atoms). In our calculations, we have used standard PPP parameters, $t_0 = -2.40$ eV and $U = 11.26$ eV, that have been widely used over the past several decades^{64,65}; the employed on-site correlation energy U is the sum of the ionization potential and the electron affinity of C in a sp^2 -hybridized system⁶⁴. Substitution effects can be probed by introducing positive or negative site energies ϵ_i , for mimicking donor and acceptor groups respectively, while the site energy for unsubstituted C-atoms is taken as zero.

B. The DMRG Technique

In the DMRG technique, the full system is divided into two blocks, generally referred to as the left (L) and right (R) blocks, which are iteratively grown by a few sites (usually one) at each step. The complete wavefunction of the system is represented in the direct product space of the block states. The block space of each individual block is approximated by retaining reduced density matrix eigenvectors of the corresponding block with highest eigenvalues and the exponentially growing Hilbert space of a many-body system gets well-adapted into a basis space of fixed dimension, independent of the system size. The reduced density matrix of a particular block is obtained by employing full system eigenstates while assuming the other block as environment, followed by its diagonalization to obtain the block states. Matrices of the block Hamiltonians and of the individual site operators are constructed at the ' l '-th step in the direct product basis of old block states (obtained in the step ' $l-1$ ') and Fock states of the newly added sites. Afterwards, these matrices are renormalized employing the new block states constructed at the ' l '-th step. In the next step, the system is grown by adding a few sites to both the left and right blocks and the full system Hamiltonian is constructed in the direct product basis of the block states of the left and right blocks along with the Fock states of the newly added sites. The full Hamiltonian matrix is diagonalized to obtain targeted eigenstates of the system

TABLE I. Ground and lowest optical state energies of coronene within the non-interacting Hückel model, in units of t_0 , calculated using the Hückel and symmetrized DMRG approaches.

Nature of the state	Hückel	Symmetrized DMRG
Ground state	-34.57183	-34.51000
Optical state	-33.49345	-33.36570

which are then used to study different physical properties. The above procedure, known as the infinite DMRG method, is iteratively repeated until the desired system size is reached.

Although the infinite DMRG algorithm can be employed to study physical properties at the polymeric limit, for finite-size systems, the accuracy of the calculation can be significantly improved by the finite DMRG algorithm. In the infinite scheme, the block states at the intermediate steps do not correspond to the final system. This flaw can be resolved through construction of block spaces employing wavefunctions corresponding to the final system size. The procedure is termed as ‘sweeping’, where iteratively one block is grown at the expense of the other block, while keeping the final system size fixed. At the final step of a full-sweep, the sizes of the two blocks become $N/2 - 1$ where, N is the final system size. The finite DMRG procedure is a non-trivial but essential procedure for the study of molecular systems as the energies improve significantly following the sweeping procedure.

For quasi-one dimensional systems, the order in which the new sites are added to build the molecule is important to attain high accuracy. For the same DMRG cut-off, different sequences of adding new sites give different energy eigenvalues. This is well known in the ab initio DMRG approaches where the order of adding orbitals is determined by the entanglement⁶⁶⁻⁶⁸. The order in which the sites are added to build the molecule coronene and its derivative is as follows. At every stage of the infinite DMRG iteration, transfer terms are introduced between the sites added earlier (old sites) and the new sites as well as between old sites in the two blocks. We add the sites in such a way that the interaction between the old site and the new site at any given stage involves as recent an old site as possible. This implies that the interaction between the new site and the old site is such that the old site operators have been renormalized the fewest number of times possible. In the early DMRG studies of systems with periodic boundary condition, this particular requirement is restored by placing one of the newly added sites between the old blocks while placing the other new site at the end of a particular old block (L or R).

Fig. 1 shows the steps of building the coronene molecule starting from a four-atom ring and adding two new atoms at each step. The noninteracting Hückel model for this molecule ($\epsilon_i = U = V_{ij} = 0$ in Eq. 1)

can be solved trivially for ground and low-lying excited states. The same can also be obtained using the DMRG algorithm. Comparison of the two results (see Table. I) provides a stringent check on the DMRG accuracy, since within the noninteracting model, the system block and the environment block are more entangled, as compared to interacting models with site-diagonal interactions, such as the Hubbard and the PPP models⁶⁹. We find that for coronene, the ground state energy is accurate to 0.17% and the optically excited state is accurate to 0.38% while the optical gap (energy difference between the two) is accurate to 6.1% (exact gap is $1.07838t_0$). Since the accuracy of the DMRG method increases with decreasing entanglement, the Hückel model provides an upper limit for the errors in the correlated models. Additionally, the comparison of the DMRG calculations against the Hückel model can be employed as an effective tool to calibrate the required block space dimension for desired numerical accuracy within these finite-size quasi-one dimensional systems.

C. Symmetries of the Hamiltonian

We are particularly interested in the low-energy one and two-photon excited states along with the low-lying triplet states of the molecules. However, the number of energy states that reside between the ground state and the desired states can be variable and large. Hence, targeting ‘important’ states is an almost impossible task without invoking the basic symmetries of the full Hamiltonian. In the present study, we have utilized the end-to-end interchange symmetry (C_2), e - h symmetry and spin-flip or parity symmetry (P) of the full system Hamiltonian within the DMRG framework employing a modified algorithm for symmetry adaptation⁷⁰. In this algorithm, the symmetry operators are expressed as extremely sparse matrices, with only one non-zero element per row and column. Consequently, we get rid of the computationally expensive Gram-Schmidt orthonormalization procedure during the construction of the symmetry adapted basis states.

The PPP Hamiltonian conserves total spin (S), but it is difficult to adopt total spin conservation within the DMRG scheme. In order to target states with different S , we exploit the spin-flip symmetry (P) in the $S_z = 0$ sector, where the Hamiltonian remains invariant as all spins of the system are reversed. The symmetry bifurcates the $S_z = 0$ space into one subspace with even total spin (designated as ‘e’) and another with odd total spin (designated as ‘o’). In addition, the Hamiltonian for a neutral bipartite system remains invariant under e - h symmetry, where the creation (annihilation) operator of one sub-lattice is interchanged by annihilation (creation) operator, while in the other sub-lattice, the interchange accompanies a phase factor of -1 . The eigenstates can be labeled ‘+’ or ‘-’ depending upon the eigenvalue ($+1$ or -1) while operated by e - h symmetry operator. Fi-

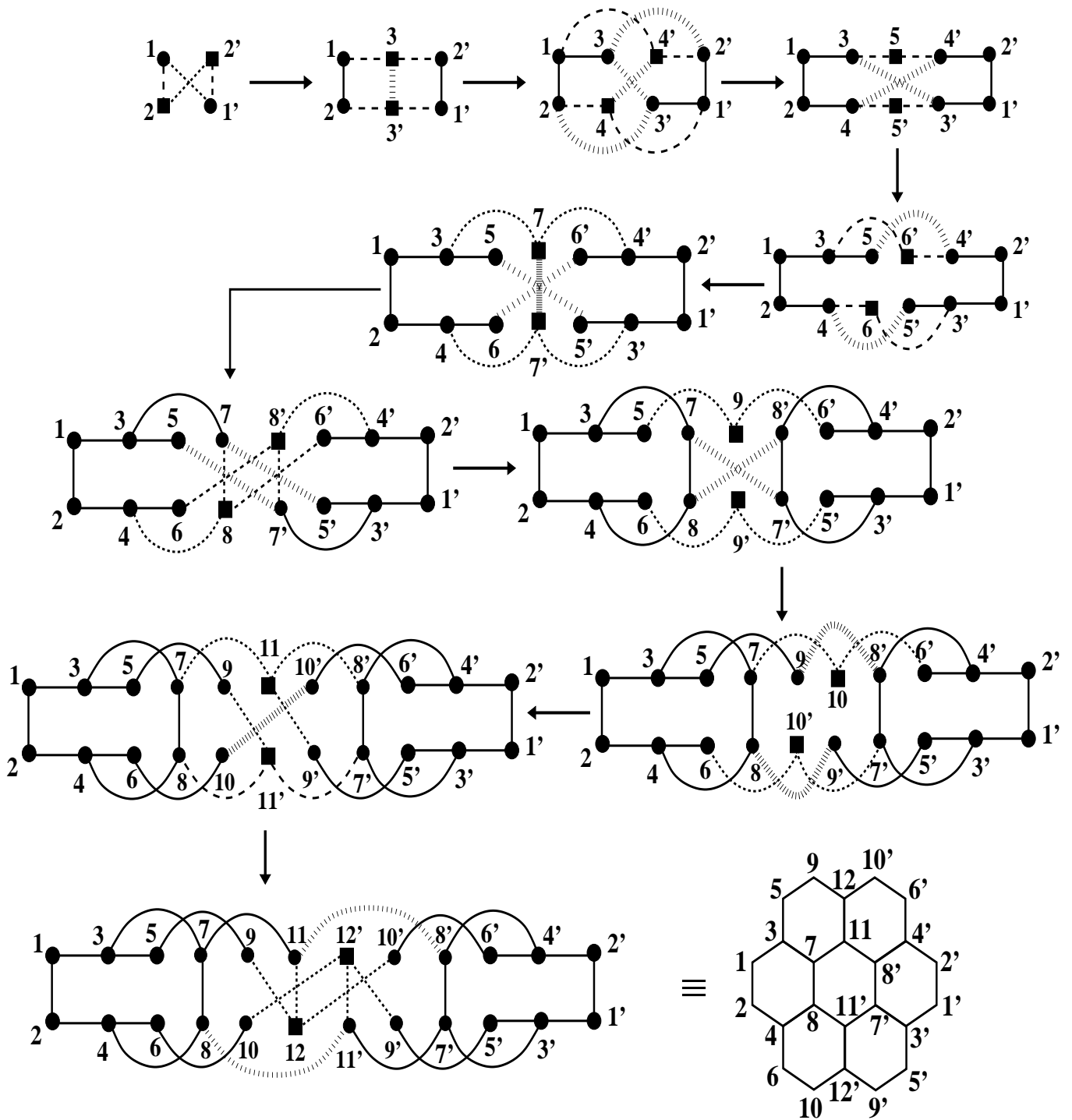


FIG. 1. Construction of coronene molecule in the infinite DMRG method starting from a small system (4 sites). The number of connections between the new and the old sites at the intermediate steps are kept similar to that in the final system for higher accuracy. At every step of the algorithm two new sites are added, one to the system block (L) and other to the environment block (R). The sites in the L -block are denoted by unprimed numbers while those in the R -block are denoted by primed numbers. The newly added sites are denoted by filled square (■) while old sites are denoted by filled circles (●). Solid lines are bonds within a block. The broken lines denote the connections between ● and ■. Bonds between the two blocks as well as the bond between newly added sites are denoted by hatched lines.

nally, the full system eigenstates can be labeled A or B , based on their parity (even or odd) with respect to C_2 operation.

The three symmetry operators and their products along with identity form an Abelian group which subdivides the $S_z = 0$ space into eight subspaces. In general, the ground state has even character with respect to every symmetry operation and lies in the ${}^eA^+$ subspace. Optical one-photon states remain in ${}^eB^-$ space while the two-photon states have the same symmetry characters as the ground state. The lowest triplet state energy is in the $S_z = 1$ space where the P symmetry cannot be employed and it remains in the B^+ space.

In each symmetry subspace, we have calculated a few low-lying eigenstates of the Hamiltonian to ascertain the spectra in the low energy region. However, for the calculation of the transition dipole moments, the average reduced density matrix is employed instead of the reduced density matrix corresponding to a single state, in order to attain a common block space description. The average reduced density matrix²⁶ is defined by $\rho = \sum_i \omega_i \rho_i$ where ρ_i is the reduced density matrix corresponding to eigenstates $|i\rangle$. ω_i are the weights of the corresponding eigenstates, which we have taken as $\omega_i = 1/W$, where W is the number of low-lying eigenstates computed in the symmetry subspace. The block states obtained from the average reduced density matrix are employed for the DMRG calculations. The magnitude of the cut-off in the block space dimension does not lead to admixture of the different symmetry states in the state-average DMRG calculations, since we have retained all symmetry partners of the block states in our algorithm.

D. Two-Photon Absorption Cross-Section

Two-photon absorption (TPA) is a third order nonlinear optical process which involves simultaneous absorption of two photons and is related to the imaginary part of the second order hyperpolarizability $\chi^{(3)}(-\omega; \omega, -\omega, \omega)$, where $\hbar\omega$ is half of the excitation energy of the two-photon state $|TP\rangle$ ($\hbar\omega = (E_{TP} - E_G)/2$). We have employed the correction vector (CV) technique for computing the TPA cross-section. The first order CV is calculated employing the inhomogeneous linear algebraic equation,

$$(\hat{H} - E_G + \hbar\omega)|\phi_i^{(1)}(\omega)\rangle = \tilde{\mu}_i|G\rangle \quad (3)$$

where H is the Hamiltonian matrix, $|G\rangle$ is the ground state with energy E_G and $\tilde{\mu}_i$ is the i -th component of the dipole displacement operator, $\tilde{\mu}_i = \hat{\mu}_i - \langle G|\hat{\mu}_i|G\rangle$ ($i = x, y, z$). The linear algebraic equations are solved efficiently employing the small matrix algorithm developed by Ramasesha⁷¹. On expansion in the basis of the excited states $\{|R\rangle\}$, the correction vector can be written

as,

$$|\phi_i^{(1)}(\omega)\rangle = \sum_R \frac{\langle R|\tilde{\mu}_i|G\rangle}{E_R - E_G + \hbar\omega}|R\rangle \quad (4)$$

The expression for the ij -th element of the two-photon transition matrix is given by⁷²,

$$\begin{aligned} S_{ij}(\omega) &= \sum_R \left[\frac{\langle G|\tilde{\mu}_i|R\rangle\langle R|\tilde{\mu}_j|TP\rangle}{E_R - E_G - \hbar\omega} + \frac{\langle G|\tilde{\mu}_j|R\rangle\langle R|\tilde{\mu}_i|TP\rangle}{E_R - E_G - \hbar\omega} \right] \\ &= \langle \phi_i^{(1)}(-\omega)|\tilde{\mu}_i|TP\rangle + \langle \phi_j^{(1)}(-\omega)|\tilde{\mu}_i|TP\rangle \end{aligned} \quad (5)$$

while, the TPA cross-section for a linearly polarized monochromatic light of a randomly oriented sample as in solution or gas phase is given by⁷²,

$$\delta_{TPA} = \frac{1}{15} \sum_{i,j=x,y,z} (S_{ii}S_{jj}^* + 2S_{ij}S_{ij}^*) \quad (6)$$

III. COMPUTATIONAL RESULTS

We have studied a few low-lying states of coronene in different symmetry subspaces within the PPP model and the relevant energy gaps, defined as differences from the ground state, are tabulated in Table II. We have also calculated energies in the corresponding symmetry subspaces for the substituted coronene of Fig. 2 (see Table. III), with donor and acceptor groups of equal strength ($|\epsilon| = 1.0$ eV). For all our calculations, we maintained truncated block space dimension of ~ 1000 . We have used a single spatial symmetry, the C_2 symmetry whose axis is perpendicular to the molecular plane, as our DMRG calculation cannot handle more than one symmetry axis. We label all the eigenstates using the D_{2h} subgroup symmetry, which is simpler than determining the irreducible representations of the D_{6h} point group symmetry. In the D_{6h} point group representation, allowed optical transitions from the ground state with A_{1g} symmetry are only to doubly degenerate E_{1u} states whose transition dipoles lie in the molecular plane. In the D_{2h} subgroup, these states remain as two-fold degenerate B_{2u} and B_{3u} states respectively, but now their transition dipoles lie strictly along orthogonal y - and x -axes respectively. Consequently, use of D_{2h} symmetry subgroup instead of D_{6h} simply implies that the doubly degenerate optical states, with mixed polarizations in the molecular plane, are assumed to have distinct polarizations along the Cartesian axes and *no information has been lost*. Within the DMRG calculations of these doubly degenerate states, however, calculated transition dipoles along any one direction, picks up a weak orthogonal component even when D_{2h} symmetry is employed. The lowest optical states obtained may not be the states with highest transition dipole moment, which will be prominent in UV-visible spectroscopy but corresponds to the lowest energy state of the appropriate symmetry subspace²³.

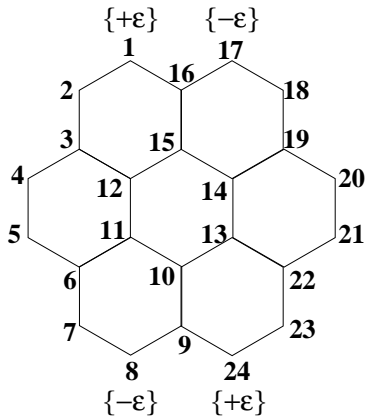


FIG. 2. (Color online) Schematic diagram of coronene molecule. The sites of substitution in substituted coronene are also indicated; $+\epsilon$ represents a donor site while $-\epsilon$ represents an acceptor site.

A. Correlation Strength and Ordering of Excited States

As has been shown explicitly in calculations of linear polyenes^{2,73–75}, the most important consequence of strong electron correlations is the energy ordering of excited states according to their *ionicities*. In the language of valence bond (VB) theory, eigenstates are covalent if they are dominated by VB diagrams in which the p_z orbitals of C-atoms are neutral, *i.e.*, singly occupied. Similarly, eigenstates are ionic if in the dominant VB diagrams, there occur at least one pair of p_z orbitals that are positively and negatively charged. One simple measure of the ionicity within the PPP Hamiltonian of Eq. (1), is the expectation value of $\langle n_{i,\uparrow}n_{i,\downarrow} \rangle$, which measures the probability of double occupancy in the p_z orbital at site i . Within the noninteracting Hückel model, $\langle n_{i,\uparrow}n_{i,\downarrow} \rangle$ is exactly 0.25 for the ground state. The ground state of the interacting Hamiltonian is more covalent than that of the noninteracting Hamiltonian and $\langle n_{i,\uparrow}n_{i,\downarrow} \rangle < 0.25$ for the former. Experimentally, the ionicities of the excited states is a more relevant quantity. Within the noninteracting model, there is no one-to-one correspondence between energies of states and their ionicities. Within the interacting model, however, predominantly covalent states occur energetically below predominantly ionic states.

Fortunately, this relative ordering, lowest covalent excited states occurring below lowest ionic states, can be tested optically in centrosymmetric systems with distinct one-photon and two-photon states. As was recognized long back, dipole selection rules in centrosymmetric systems dictate that transition dipole matrix elements are nonzero only between states with opposite parity and $e-h$ symmetries^{2,85}. In the context of neutral π -conjugated molecules, this means that one-photon transition from the even parity eA^+ covalent ground state can occur only to odd parity eB^- states. Note that, this also im-

plies that the lowest two-photon states, which are dipole-coupled to the eB^- states are covalent (see Eq. (5)), and are hence likely to occur below the lowest one-photon state. The occurrence of the lowest two-photon state below the lowest one-photon state has been experimentally confirmed in linear polyenes⁷³.

The theoretical measure of the correlation strength for a charge-neutral C-based molecule to a first approximation is the ratio of the effective on-site correlation, to the width of the one-electron energy spectrum. The effective onsite correlation within the PPP model is $U_{PPP} \sim (U - V_{12})$, where V_{12} is the nearest-neighbor Coulomb interaction. This quantity is independent of dimensionality. In contrast, the width of the one-electron energy spectrum increases with dimensionality, implying therefore that the effective correlation strength is smaller in two dimension than in one dimension. The relative energies of the lowest one versus two-photon states in graphene nanofragments can therefore not be guessed based on the known results for polyenes.

Aside from its covalent nature, another aspect of the lowest two-photon state in linear polyenes has been of interest, *viz.*, its characterization as a bound state of the two lowest triplet excitations T_1 of the polyene^{6,75}. Indeed, several of the lowest two-photon states in linear polyenes are superpositions of triplet excitations T_1 as well as higher energy T_2 , T_3 etc. (the two triplets that constitute an excited covalent singlet need not be identical)⁶. In other words, even parity covalent excited states in linear polyenes are necessarily superpositions of two triplets. It is not a priori clear that this will hold true in polycyclic aromatic hydrocarbons such as coronene, where there occur C-atoms that are different, peripheral versus internal, as well as bi-coordinate versus tri-coordinate.

In Table II, we have listed the energies of the lowest optical states, the lowest triplet states and the lowest two-photon states, relative to the ground state. We have also included the lowest states that are optically dark under both one- and two-photon excitation. The latter are equivalent to the covalent B_u^+ states of polyenes⁷⁵, each of which can be viewed as superposition of covalent B_u triplets T_i and T_j , $i \neq j$. Because of our use of a single C_2 symmetry element, we are unable to distinguish between A_g^+ and B_{1g}^+ states that are degenerate in the noninteracting limit but are nondegenerate within the correlated PPP Hamiltonian²³. The ${}^1B_{2u}^-$ and ${}^1B_{3u}^-$ states are degenerate, but the triplet states ${}^3B_{2u}^+$ and ${}^3B_{3u}^+$ need not to be degenerate in coronene²³. We have therefore assigned the triplet at 2.35 eV to ${}^1{}^3B_{2u}^+ / {}^1{}^3B_{3u}^+$, while the one at 3.0 eV is assigned to ${}^1{}^3B_{3u}^+ / {}^1{}^3B_{2u}^+$. We have given similar labels to the lowest two-photon states, where two multiple assignments are possible.

The lowest two-photon energy along with the lowest triplet energy calculated in coronene are in excellent agreement with the previously reported values by Aryanpour et al., obtained using the MRSDCI technique²³. The calculated energy of the lowest two-photon state

TABLE II. Energies of low-lying two-photon states, optical states, triplet states and a few other optically dark states in coronene, relative to the ground state. Although coronene has D_{6h} symmetry, here the states are labeled by the symmetry representations of its subgroup D_{2h} . Whenever a state cannot be uniquely labeled due to lower symmetry employed in the study, both possible labels for the state have been given. The transition dipole moment (in Debye) from ground state to the excited states ($\mu_{tr,x/y}$) along specific axes are also specified in the last two columns. Energies determined by the UV-visible spectroscopy are also mentioned in the footnotes (a) and (c).

Coronene				
Nature of the state	State	Energy Gap (eV)	$\mu_{tr,x}(D)$	$\mu_{tr,y}(D)$
Two-photon	$(2^1A_g^+/1^1B_{1g}^+)$	3.97	0.00	0.00
	$(1^1B_{1g}^+/2^1A_g^+)$	4.09	0.00	0.00
	$(3^1A_g^+/2^1B_{1g}^+)$	5.08	0.00	0.00
Optical	$1^1B_{2u}^-$	4.83 ^a	0.81 ^b	8.43
	$1^1B_{3u}^-$	4.87 ^a	7.51	0.49 ^b
Triplet	$(1^3B_{2u}^+/1^3B_{3u}^+)$	2.35 ^c	0.00	0.00
	$(1^3B_{3u}^+/1^3B_{2u}^+)$	3.00	0.00	0.00
	$(2^3B_{2u}^+/2^3B_{3u}^+)$	3.02	0.00	0.00
	$(1^3A_g^+/1^3B_{1g}^+)$	3.35	0.00	0.00
Dark states	$(1^1B_{2u}^+/1^1B_{3u}^+)$	2.82	0.00	0.00
	$(1^1A_g^-/1^1B_{1g}^-)$	3.88	0.28	1.74
	$(1^1B_{1g}^-/1^1A_g^-)$	4.73	0.00	0.00

^a 4.10 eV²³; 4.06 – 4.27 eV⁷⁶; 4.21 eV⁷⁷; 4.07 – 4.23 eV⁷⁸; 4.12 – 4.44 eV⁷⁹; 4.06 – 4.27 eV⁸⁰; 4.28 eV⁸¹; 4.06 eV⁸²; 4.09 eV⁸³; 4.27 eV⁸⁴.

^b Non-zero value of transition dipole moment along polarization direction forbidden by symmetry is an artifact of the calculations as average density matrices, calculated from eigenstates of different symmetry subspaces, are employed to determine the transition dipole moment. However, the errors are negligible as intensities depend on the square of the transition dipole moment.

^c 2.40 eV^{81,83}.

(that occurs in the $1^1A_g^+$ subspace) reported earlier is 3.96 eV for coronene, to be compared against 3.97 eV found in our calculations. These numbers match very well against the experimental two-photon absorption spectrum²³. The earlier reported lowest triplet energy is 2.38 eV (experimentally identified peak is at \sim 2.40 eV, probed by phosphorescence and electron energy loss spectroscopy^{81,83}), which is also close to 2.35 eV obtained by us. However, the lowest one-photon energy and relative position of the lowest optical state with respect to the lowest two-photon state do not agree well with the earlier study^{23,24}. In coronene, the energy of the lowest optical $1^1B_{2u}^-$ and $1^1B_{3u}^-$ states calculated earlier^{23,24} is 4.11 eV while we have found two nearly degenerate excitations at higher energies 4.83 and 4.87 eV, respectively.

The experimental linear absorption spectrum of coronene shows a prominent absorption band in this region with maximum at 4.06 – 4.30 eV both in solution^{23,76–80,86} and vapor phase^{81–84}. The discrepancy between our result and the previous computational result arises from the use of “bare” PPP-Ohno parameters in the present work as opposed to “screened” parameters in the previous work^{23,24}.

We see in Table II a low-lying state at an energy of

3.88 eV, with a small transition dipole moment. This state was found to be optically forbidden in the MRS-DCI calculations^{23,24}. The weak dipole coupling found in the present calculations probably results from our incorporation of only one C_2 symmetry axis or our use of the average density matrices, obtained from eigenstates of different symmetry subspaces, that can lead to weak spatial symmetry violation. Indeed, we revisited the calculations without employing the C_2 symmetry and found the energy of this state remains unchanged. However, this state lies in the ‘-’ subspace of $e-h$ symmetry with a small transition dipole moment. Therefore, we conclude that this state corresponds to the $1^1A_g^-/1^1B_{1g}^-$ state and in agreement with the previous study^{23,24}. The calculated small transition dipole moment is thus an artifact, although weak violation of $e-h$ symmetry, as would occur in the real molecule, can lead to observable absorption. Indeed, as pointed out in the earlier theory-experiment work²³, this “forbidden” state is seen as a weak absorption experimentally.

The 2.82 eV excitation in coronene, on the other hand, is strictly forbidden as it belongs to the same $e-h$ symmetry subspace as the ground state. This argument is supported by the fact that this state acquires some inten-

TABLE III. Energies of low-lying states in substituted coronene are tabulated below. The transition dipole moment (in Debye) from ground state to the excited states ($\mu_{tr,x/y}$) along specific axes are also specified in the last two columns.

Substituted coronene				
Nature of the state	State	Energy Gap (eV)	$\mu_{tr,x}(D)$	$\mu_{tr,y}(D)$
Two-photon	2^1A_g	4.01	0.00	0.00
	3^1A_g	4.81	0.00	0.00
	4^1A_g	4.90	0.00	0.00
Optical	1^1B_u	2.90	0.00	0.23
	2^1B_u	3.87	0.12	1.46
	3^1B_u	5.18	0.17	7.52
	4^1B_u	5.97	4.10	0.59
Triplet	1^3B_u	2.29	0.00	0.00
	2^3B_u	2.92	0.00	0.00
	3^3B_u	3.48	0.00	0.00

sity on breaking the $e-h$ symmetry by introducing substituents, as can be seen from Table. III. Appearance of absorption peak at ~ 2.95 eV in thin films of coronene also suggest presence of a singlet state close to the lowest triplet state^{87,88}.

Substitution by donor-acceptor groups does not seem to have appreciable effect on the energy gaps between the states, although the lifting of $e-h$ symmetry allows optical transitions to states which are dipole-forbidden in the unsubstituted molecule. The extent of mixing of different symmetry states of the unsubstituted system due to substitution depends on the strength of the donor-

acceptor groups.

The spin gap (energy difference between lowest triplet state and ground state) is also a good measure of the effective correlation strength. Stronger the effective correlation, the smaller is the spin gap. Based on the similar spin gaps in the unsubstituted versus substituted molecules, we conclude that the effective correlation strengths are the same in the two molecules. This indicates that the previous claim of stronger correlation effect in lower symmetry molecules²⁴ may be an oversimplification.

In Fig. 3 we have plotted the $\langle n_{i,\uparrow}n_{i,\downarrow} \rangle$ for each of the C-atoms in coronene, for the ground state, the optical $1^1B_{2u}^-$ and $1^1B_{3u}^-$ states, the lowest two-photon state at 3.97 eV, and the lowest triplet state. As expected, $\langle n_{i,\uparrow}n_{i,\downarrow} \rangle$ for the ground state is smaller than 0.25 for all C-atoms, indicating its covalent character. The same expectation value is larger for the optical state, also as anticipated for this ionic state. Interestingly, $\langle n_{i,\uparrow}n_{i,\downarrow} \rangle$ for the lowest triplet and the lowest two-photon state are both *smaller* than that of the ground state, indicating, (i) covalent character larger than that of the ground state, and (ii) nearly equal covalent character in both. The equality between the lowest triplet and the lowest two-photon state is surprising, given that the latter is not a simple two-triplet state.

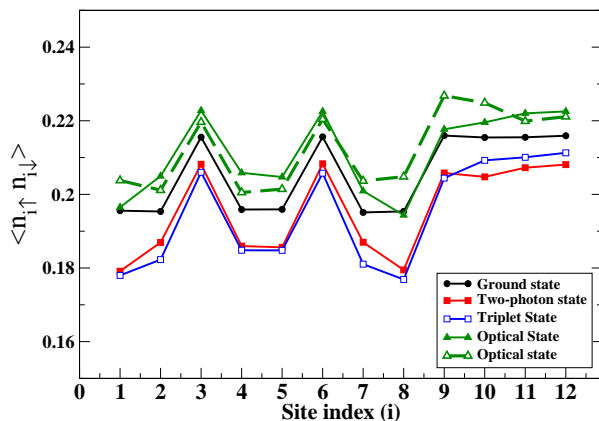


FIG. 3. (Color online) The probability of double occupancy of C-atoms by electrons plotted against site index (see Fig. 2) for coronene. Sites related by C_2 symmetry are perfectly equivalent and hence are not shown. Lines are guides to the eye only. The two different plots for the optical states correspond to the two nearly degenerate states.

B. TPA cross-section

In Table. IV, we have tabulated the TPA cross-sections for low-lying two-photon states in coronene along with two-photon transition matrix elements. In coronene, we find that the higher energy two-photon state $3^1A_g^+/2^1B_{1g}^+$ has larger TPA cross-section than that of

TABLE IV. Two-photon transition matrix elements along with TPA cross-section for lowest two-photon states in unsubstituted coronene molecule. Possible symmetry labels are provided wherever unique symmetry label cannot be determined. Transition matrix elements as well as TPA cross-sections are given in atomic units.

	Two-photon state	S_{xx}	S_{yy}	S_{xy}	δ_{TPA}
Coronene	$(2^1A_g^+/1^1B_{1g}^+)$	10.68	-67.05	-0.97	821.56
	$(1^1B_{1g}^+/2^1A_g^+)$	1.94	-0.97	-35.95	349.39
	$(3^1A_g^+/2^1B_{1g}^+)$	23.32	-69.96	1.94	868.77

the lowest two-photon states. This theoretical result is in qualitative agreement with the experimental solution two-photon measurements in this energy region. Since the two Cartesian axes are equivalent in coronene, the transition matrix elements S_{xx} and S_{yy} should be nearly same. However, in our calculations, we found $|S_{yy}| > |S_{xx}|$ in most of the cases, which we attribute to the fact that we have used only one C_2 symmetry axis while targeting the states as well as to the use of average density matrices. When the states are nearly degenerate, these approximations could break the true symmetry which the eigenstates will otherwise possess.

IV. DISCUSSION AND CONCLUSION

We have studied the lowest energy states and their relative orderings in two finite centrosymmetric graphene nanoflakes within the PPP π -electron Hamiltonian, using the DMRG approach. Electron correlations drive covalency in both molecules and also change the relative orderings of one- versus two-photon excitations. As in linear polyenes, the lowest triplet and the lowest two-photon states are covalent in the language of VB theory, and occur below the lowest one-photon optical state. The proximity in energy between the ionic one-photon state and the covalent two-photon state, relative to that in the polyenes, however is an indication of relatively weaker correlation effect in these two-dimensional molecules with wider one-electron energy spectrum. Additionally, the lowest two-photon state is not a simple two-triplet state, unlike in the polyenes. We believe that this is a consequence of different topology in these polycyclic hydrocarbons, in which there occur C-atoms with both two and three nearest neighbors. The occurrence of higher energy two-photon states that are two-triplets²⁴ indicates that in these two-dimensional molecules there occur two different kinds of covalent states, which may or may not be simply classified as two-triplet. This relationship between the natures of covalent states with topology, along with the correlation effects in graphene fragments of larger and larger size, are topics of ongoing and future interest.

ACKNOWLEDGMENTS

The authors are grateful for financial support from the Indo-US Science and Technology Forum that was instrumental in the creation of a Joint Center, which made this collaborative research possible. SR is thankful to the Department of Science and Technology, India for financial support. SM acknowledges partial support from U. S. NSF grants CHE-1764152 and the UA-REN Faculty Exploratory Research Grant. SP acknowledges CSIR India for a senior research fellowship.

- ¹H. Zhao and S. Mazumdar, Phys. Rev. Lett. **93**, 157402 (2004).
- ²B. S. Hudson, B. E. Kohler, and K. Schulten, *Excited States*, edited by E. C. Lim, Vol. 6 (Academic Press, New York, 1982) p. 1.
- ³Z. G. Soos and S. Ramasesha, Phys. Rev. B **29**, 5410 (1984).
- ⁴P. Tavan and K. Schulten, J. Chem. Phys. **70**, 5407 (1979).
- ⁵P. Tavan and K. Schulten, J. Chem. Phys. **70**, 5414 (1979).
- ⁶P. Tavan and K. Schulten, Phys. Rev. B **36**, 4337 (1987).
- ⁷P. Tavan and K. Schulten, J. Chem. Phys. **85**, 6602 (1986).
- ⁸Z. G. Soos, S. Ramasesha, and D. S. Galvao, Phys. Rev. Lett. **71**, 1609 (1993).
- ⁹D. Baeriswyl, D. K. Campbell, and S. Mazumdar, *Conjugated Conducting Polymers*, edited by H. Kiess, Springer Series in Solid-State Sciences, Vol. 102 (Springer, Berlin, 1992).
- ¹⁰Z. Shuai, D. Beljonne, R. J. Silbey, and J. L. Brédas, Phys. Rev. Lett. **84**, 131 (2000).
- ¹¹T. Yamamoto, T. Noguchi, and K. Watanabe, Phys. Rev. B **74**, 121409 (2006).
- ¹²B. M. Wong, J. Phys. Chem. C **113**, 21921 (2009).
- ¹³G. Mallocci, G. Cappellini, G. Mulas, and A. Mattoni, Chemical Physics **384**, 19 (2011).
- ¹⁴C. D. Spataru, S. Ismail-Beigi, L. X. Benedict, and S. G. Louie, Phys. Rev. Lett. **92**, 077402 (2004).
- ¹⁵E. Chang, G. Bussi, A. Ruini, and E. Molinari, Phys. Rev. Lett. **92**, 196401 (2004).
- ¹⁶L. Yang, J. Deslippe, C.-H. Park, M. L. Cohen, and S. G. Louie, Phys. Rev. Lett. **103**, 186802 (2009).
- ¹⁷Y.-W. Son, M. L. Cohen, and S. G. Louie, Nature **444**, 347 (2006).
- ¹⁸M. Schreiber, M. R. Silva-Junior, S. P. A. Sauer, and W. Thiel, J. Chem. Phys. **128**, 134110 (2008).
- ¹⁹M. R. Silva-Junior, M. Schreiber, S. P. A. Sauer, and W. Thiel, J. Chem. Phys. **133**, 174318 (2010).
- ²⁰J. H. Starcke, M. Wormit, J. Schirmer, and A. Dreuw, Chem. Phys. **329**, 39 (2006).
- ²¹S. Knippenberg, D. R. Rehn, M. Wormit, J. H. Starcke, I. L. Rusakova, A. B. Trofimov, and A. Dreuw, J. Chem. Phys. **136**, 064107 (2012).
- ²²C. M. Krauter, M. Pernpointner, and A. Dreuw, J. Chem. Phys. **138**, 044107 (2013).

- ²³K. Aryanpour, A. Roberts, A. Sandhu, R. Rathore, A. Shukla, and S. Mazumdar, *J. Phys. Chem. C* **118**, 3331 (2014).
- ²⁴K. Aryanpour, A. Shukla, and S. Mazumdar, *J. Chem. Phys.* **140**, 104301 (2014).
- ²⁵S. R. White, *Phys. Rev. Lett.* **69**, 2863 (1992).
- ²⁶S. R. White, *Phys. Rev. B* **48**, 10345 (1993).
- ²⁷U. Schollwöck, *Rev. Mod. Phys.* **77**, 259 (2005).
- ²⁸K. A. Hallberg, *Adv. Phys.* **55**, 477 (2006).
- ²⁹S. Ramasesha, S. K. Pati, Z. Shuai, and J. L. Brédas, *Advances in Quantum Chemistry*, edited by J. R. Sabin, M. C. Zerner, and E. Brändas, Vol. 38 (Academic Press, San Diego, 2000) pp. 121–215.
- ³⁰P. R. Wallace, *Phys. Rev.* **71**, 622 (1947).
- ³¹H. Min, B. Sahu, S. K. Banerjee, and A. H. MacDonald, *Phys. Rev. B* **75**, 155115 (2007).
- ³²E. K. Yu, D. A. Stewart, and S. Tiwary, *Phys. Rev. B* **77**, 195406 (2008).
- ³³P. Gava, M. Lazzeri, A. M. Saitta, and F. Mauri, *Phys. Rev. B* **79**, 165431 (2009).
- ³⁴G. Giovannetti, P. A. Khomyakov, G. Brocks, P. J. Kelly, and J. van den Brink, *Phys. Rev. B* **76**, 073103 (2007).
- ³⁵Z. H. Ni, T. Yu, Y. H. Lu, Y. Y. Wang, Y. P. Feng, and Z. X. Shen, *ACS Nano* **2**, 2301 (2008).
- ³⁶R. M. Ribeiro, N. M. R. Peres, J. Coutinho, and P. R. Briddon, *Phys. Rev. B* **78**, 075442 (2008).
- ³⁷S. Latil and L. Henrard, *Phys. Rev. Lett.* **97**, 036803 (2006).
- ³⁸C. Feng, C. S. Lin, W. Fan, R. Q. Zhang, and M. A. Van Hove, *J. Chem. Phys.* **131**, 194702 (2009).
- ³⁹T. B. Martins, R. H. Miwa, A. J. R. da Silva, and A. Fazzio, *Phys. Rev. Lett.* **98**, 196803 (2007).
- ⁴⁰B. Xu, Y. H. Lu, Y. P. Feng, and J. Y. Lin, *J. Appl. Phys.* **108**, 073711 (2010).
- ⁴¹S. Sanyal, A. K. Mannaa, and S. K. Pati, *J. Mater. Chem. C* **2**, 2918 (2014).
- ⁴²J. A. Fürst, T. G. Pedersen, M. Brandbyge, and A.-P. Jauho, *Phys. Rev. B* **80**, 115117 (2009).
- ⁴³H. Tachikawa, Y. Nagoya, and H. Kawabata, *J. Chem. Theory Comput.* **5**, 2101 (2009).
- ⁴⁴V. Barone, O. Hod, J. E. Peralta, and G. E. Scuseria, *Acc. Chem. Res.* **44**, 269 (2011).
- ⁴⁵W. L. Wang, S. Meng, and E. Kaxiras, *Nano Lett.* **8**, 241 (2008).
- ⁴⁶W. L. Wang, O. V. Yazyev, S. Meng, and E. Kaxiras, *Phys. Rev. Lett.* **102**, 157201 (2009).
- ⁴⁷M. Ezawa, *Phys. Rev. B* **76**, 245415 (2007).
- ⁴⁸J. Fernández-Rossier and J. J. Palacios, *Phys. Rev. Lett.* **99**, 177204 (2007).
- ⁴⁹W. Sheng, M. Sun, and A. Zhou, *Phys. Rev. B* **88**, 085432 (2013).
- ⁵⁰W. Sheng, M. Sun, A. Zhou, and S. J. Xu, *Appl. Phys. Lett.* **103**, 143109 (2013).
- ⁵¹A. Zhou, W. Sheng, and S. J. Xu, *Appl. Phys. Lett.* **103**, 133103 (2013).
- ⁵²S. Dutta and S. K. Pati, *J. Phys. Chem. B* **112**, 1333 (2008).
- ⁵³V. M. L. D. P. Goli, S. Prodhon, S. Mazumdar, and S. Ramasesha, *Phys. Rev. B* **94**, 035139 (2016).
- ⁵⁴C. Cocchi, D. Prezzi, A. Ruini, M. J. Caldas, and E. Molinari, *J. Phys. Chem. A* **118**, 6507 (2014).
- ⁵⁵R. Olivares-Amaya, W. Hu, N. Nakatani, S. Sharma, J. Yang, and G. K.-L. Chan, *J. Chem. Phys.* **142**, 034102 (2015).
- ⁵⁶C. Raghu, Y. A. Pati, and S. Ramasesha, *Phys. Rev. B* **66**, 035116 (2002).
- ⁵⁷S. Mukhopadhyay and S. Ramasesha, *J. Chem. Phys.* **131**, 074111 (2009).
- ⁵⁸S. Thomas, Y. A. Pati, and S. Ramasesha, *J. Phys. Chem. A* **117**, 78047809 (2013).
- ⁵⁹M. Das, *J. Chem. Phys.* **140**, 124317 (2014).
- ⁶⁰R. Pariser and R. G. Parr, *J. Chem. Phys.* **21**, 466 (1953).
- ⁶¹J. A. Pople, *Trans. Faraday Soc.* **49**, 1375 (1953).
- ⁶²K. Ohno, *Theor. Chim. Acta* **2**, 219 (1964).
- ⁶³G. Klopman, *J. Am. Chem. Soc.* **86**, 4550 (1964).
- ⁶⁴L. Salem, *The Molecular Orbital Theory of Conjugated Systems* (W. A. Benjamin, Inc., Massachusetts, 1966) p. 420.
- ⁶⁵H. Suzuki, *Electronic Absorption Spectra and Geometry of Organic Molecules* (Academic Press, New York, 1967).
- ⁶⁶S. R. White and R. L. Martin, *J. Chem. Phys.* **110**, 4127 (1999).
- ⁶⁷G. K.-L. Chan and M. Head-Gordon, *J. Chem. Phys.* **116**, 4462 (2002).
- ⁶⁸G. K.-L. Chan and M. Head-Gordon, *J. Chem. Phys.* **118**, 8551 (2003).
- ⁶⁹S. Sahoo, V. M. L. D. P. Goli, S. Ramasesha, and D. Sen, *J. Phys.:Condens. Matter* **24**, 115601 (2012).
- ⁷⁰S. Prodhon and S. Ramasesha, *Phys. Rev. B* **97**, 195125 (2018).
- ⁷¹S. Ramasesha, *J. Comput. Chem.* **11**, 545 (1990).
- ⁷²Y. Luo, P. Norman, P. Macak, and H. Ågren, *J. Phys. Chem. A* **104**, 4718 (2000).
- ⁷³B. S. Hudson and B. E. Kohler, *Chem. Phys. Lett.* **14**, 299 (1972).
- ⁷⁴K. Schulten and M. Karplus, *Chem. Phys. Lett.* **14**, 305 (1972).
- ⁷⁵S. Ramasesha and Z. G. Soos, *J. Chem. Phys.* **80**, 3278 (1984).
- ⁷⁶E. Clar, *Polycyclic Hydrocarbons*, Vol. 2 (Springer-Verlag, Berlin Heidelberg, 1964).
- ⁷⁷E. Clar and W. Schmidt, *Tetrahedron* **33**, 2093 (1977).
- ⁷⁸J. W. Patterson, *J. Am. Chem. Soc.* **64**, 1485 (1942).
- ⁷⁹J. Tanaka, *Bull. Chem. Soc. Jpn.* **38**, 86 (1965).
- ⁸⁰P. J. Stephens, P. N. Schatz, A. B. Ritchie, and A. J. McCaffery, *J. Chem. Phys.* **48**, 132 (1968).
- ⁸¹R. Abouaf and S. Díaz-Tendero, *Phys. Chem. Chem. Phys.* **11**, 5686 (2009).
- ⁸²J. Aihara, K. Ohno, and H. Inokuchi, *Bull. Chem. Soc. Jpn.* **43**, 2435 (1970).
- ⁸³K. Ohno, T. Kajiwara, and H. Inokuchi, *Bull. Chem. Soc. Jpn.* **45**, 996 (1972).
- ⁸⁴P. Ehrenfreund, L. d’Hendecourt, L. Verstraete, A. Leger, W. Schmidt, and D. Defourneau, *Astron. Astrophys.* **259**, 257 (1992).
- ⁸⁵D. Baeriswyl, D. K. Campbell, and S. Mazumdar, *Conjugated Conducting Polymers*, edited by H. Kiess, Springer Series in Solid-State Sciences, Vol. 102 (Springer, Berlin, 1992).
- ⁸⁶N. Nijegorodov, R. Mabbs, and W. Downey, *Spectrochim. Acta, Part A* **57**, 2673 (2001).
- ⁸⁷J. L. Kropp and W. R. Dawson, *J. Phys. Chem.* **71**, 4499 (1967).
- ⁸⁸A. K. Dutta, *Langmuir* **14**, 3036 (1998).